A PM-Assisted Synchronous Reluctance Motor with Two Slot-Pitch Winding

Shaohong Zhu, Tom Cox, Zeyuan Xu and Chris Gerada
Power Electronics, Machines and Control Research Group, University of Nottingham, Nottingham, UK

***Abstract*— This paper presents a novel electric motor solution to tackle the increasing demand on the traction motor for electric vehicles. The proposed electric motor has a 24 slots 10 poles fractional slot distributed winding and a PM-assisted synchronous reluctance (PMaSynR) rotor with arc-shaped barriers. First, the winding layout will be introduced. Then, a comparison with other winding layouts will be detailed. The benefits of the proposed solution including low torque ripple and high reluctance torque capability will be demonstrated. All this confirms that it is a good trade-off solution for traction application.**

***Index Terms*— electric vehicle, fractional slot distributed winding, PM-assisted synchronous reluctance motor**

I. Introduction

The electric motor is a key enabling technique in transportation electrification applications such as electric vehicles (EVs) or more electric aircraft [1]. These applications demand extremely good power/torque density, high efficiency, wide speed constant power operation and manufacturability of the electric motor as these factors will affect the range, cost and energy efficiency of the vehicle [1].

Several technology advancements in the areas of electric motor topology, high-performance steel, winding topology, and novel permanent magnet (PM), have made to improve the torque density, efficiency, and reduce costs in both manufacturing and operation [2]-[4].

Of the electric motor topologies, the induction motor and switched reluctance motor tend to be a robust and cheap solution due to their simple mechanical structure and magnet-free design. However, they suffer lower torque density, poor power factor and efficiency when compared with permanent-magnet (PM) synchronous motors [2]. Thus, the PM brushless motor is preferred in the current electric vehicle market [5].

Among the more demanding challenges for PM brushless motors designed for EV traction applications are the reluctance torque contribution, torque ripple, resistance to demagnetization, and manufacturability [1]. In this paper, a PM synchronous reluctance (SynR) motor (SynRM) associated with a novel 24 slots 10 poles (24S-10P) fractional slot distributed winding is proposed to tackle these challenges. The 24S-10P configuration was proposed for a surface-mounted permanent magnet motor in [6], which was derived from the conventional 12 slots 10 poles (12S-10P) fractional slot concentrated winding (FSCW) motor. The comparative studies of the 24S-10P with conventional 12S-10P and 90 slots 10 poles (90S-10P) were studied in [7], which suggests its advantages in terms of torque density and losses. However, the advantages in the torque ripple and reluctance torque contribution were not fully explored. In addition, the principle and inherent reason behind these advantages were not elaborated.

In this paper, the characteristics of the 24S-10P fractional slot distribution winding (FSDW) will be introduced and compared with other winding topologies with the same pole number. Then, the impact of winding topology and rotor design on the torque capability with focus on the reluctance torque and torque ripple will be revealed. Finally, to evaluate the performance expectations, a PM-assisted synchronous reluctance motor (PMaSynRM) with the 24S-10P winding layout and three other different winding topologies with the same rotor will be designed and compared.

II. Design Considerations

A. Reluctance Torque

The EM torque generated by the PM synchronous motor includes two components: magnet torque and reluctance torque. The torque equation is as below

$$T_{em} = T_{magnet} + T_{rel} \tag{1}$$

$$T_{magnet} = \frac{m}{2} P \psi_{pm} i_q \tag{2}$$

$$T_{rel} = \frac{m}{2} P \left(L_d - L_q\right) i_d i_q \tag{3}$$

As can be seen, the magnet torque T_{magnet} is related to magnet flux linkage ψ_{pm}, while the reluctance torque T_{rel} is determined by difference between L_d and L_q.

In general, if ignoring the high order winding inductance, the self- and mutual- inductance of a three-phase winding can be expressed [8][9]

$$L_{xx} = L_0 + L_2 \cos 2P\theta_r \tag{4}$$

$$M_{xy} = M_0 + M_2 \cos\left(2P\theta_r - \frac{2\pi}{3}\right) \tag{5}$$

where L_0 and M_0 are the average value of respective inductance components; L_2 and M_2 are the amplitude of cosine function of the inductance variation,

This work is funded by the INNOVATIVE doctoral programme, which is partially funded by the Marie Curie Initial Training Networks (ITN) action (project number 665468) and partially by the Institute for Aerospace Technology (IAT) at the University of Nottingham.

respectively. θ_r is the space angle of phase winding; subscript *x* and *y* denote the winding phase considered.

From winding function theory [8], the L_2 and M_2 is related to the rotor airgap length function, namely rotor saliency function in relation to θ_r.

After *d*-*q* transformation, the *d*- and *q*- inductance can be achieved as [9]

$$L_d = (L_0 - M_0) + (\frac{L_2}{2} + M_2) \quad (6)$$

$$L_q = (L_0 - M_0) - (\frac{L_2}{2} + M_2) \quad (7)$$

Thus, the reluctance torque may be written as

$$T_{em} = \frac{m}{2} P L_{diff} i_d i_q \quad (8)$$

$$L_{diff} = L_2 + 2M_2 \quad (9)$$

Therefore, to improve the reluctance torque contribution, the mutual coupling between windings, particularly M_2, plays a critical role in generating reluctance torque. That is the reason why the PMaSynRM with ISDW configuration can normally generate considerable reluctance torque compared to the same SynR rotor with FSCW configuration as FSCW configuration normally has no or very low mutual coupling between phases [10].

B. Torque Ripple

Based on the on the Lorentz force law, the instantaneous torque can be expressed as [11]

$$T_{em1} = T_{avg} + T_{ripple} \quad (10)$$

$$T_{avg} = \frac{\mu_0}{g} r l \pi P f_{s,v} f_{r,v} \sin\gamma_d \quad (11)$$

$$T_{ripple} = -\frac{\mu_0}{g} r l \pi P \sum_{\substack{v=(6k\mp1)P \\ k=1,2,3\ldots}} v f_{s,v} f_{r,v} \sin\big((v \pm P) w_r t \pm \gamma_d\big) \quad (12)$$

where r and l is the rotor radius and stack length, respectively; γ_d is the current phase advance angle; $f_{s,v}$ and $f_{r,v}$ are the amplitude of v^{th}-order stator and rotor MMF harmonic, respectively.

It can be observed that harmonic orders of the ripple torque are in multiples of six and only stator and rotor MMF harmonics with orders of $(6k\pm1)P$ can contribute to the ripple torque. On the other hand, the value of $f_{s,v}f_{r,v}$ is amplified by the space harmonic order of *v*. Thus, the high-order space harmonic may contribute disproportionally to the torque ripple amplitude.

Thus, the torque ripple features of the PMaSynRM with different winding topologies can be achieved by evaluating their stator and rotor space MMF harmonics. The PMaSynRM with conventional ISDW is expected to have a higher torque ripple due to their rich harmonics with order of $(6k\pm1)P$ [12][13].

C. Novel 24 slots 10 poles FSDW Topology

In this paper, the novel 24 slots 10 poles fractional slot distribution winding is applied to the PMaSynRM with arc-shape flux barrier rotor. With this combination, the motor can maintain a considerable reluctance torque contribution and a much lower torque ripple compared with the PMaSynRM with ISDW topology such as 30 slots 10 poles (30S-10P) and 60 slots 10 poles (60S-10P) or with FSCW such as 12 slots 10 poles (12S-10P) and 18 slots 10 poles (18S-10P). Fig. 1 shows the four PMaSynRMs with different winding topologies or slot pole combinations. More details and comparison with different winding topologies will be presented in the next section. Their slot pitch and winding factor is summarized in TABLE I.

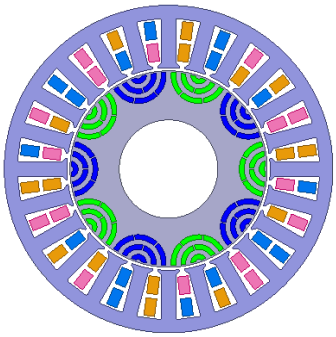

(a) Proposed 24S-10P PMaSynRM (*q*=4/5)

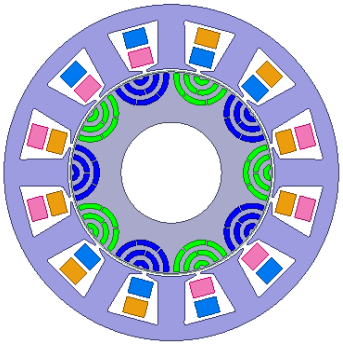

(b) 12S-10P PMaSynRM (*q*=2/5)

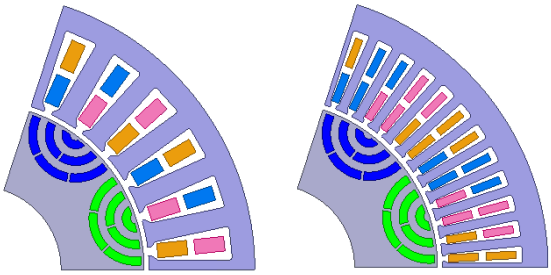

(c) 30S-10P (*q*=1) (d) 60S-10P (*q*=2)

Fig. 1. Four PMaSynRM with different winding topologies.

TABLE I
WINDING CHARACTERISTICS OF DIFFERENT SLOT-POLE COMBINATIONS

Slot-pole	*q*	Slot pitch	Synchronous winding factor k_w
24S-10P	4/5	2	0.925
12S-10P	2/5	1	0.933
30S-10P	1	2	0.866
60S-10P	2	5	0.933

III. Comparative Studies

A. Stator MMF Harmonics

Based on winding function method [8], the stator space MMF harmonics of these four winding topologies and their FFT spectrum can be plotted, as in Fig. 2. It should be noted that only those harmonics with order of $k*P$ have been plotted, although there are some fractional MMF harmonics for the windings where the q is fractional, viz., 24S-10P and 12S-10P.

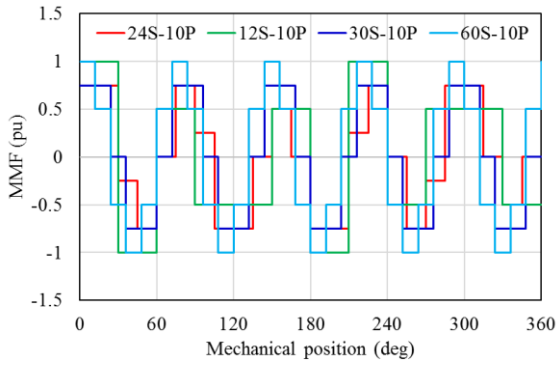

(a) MMF waveform

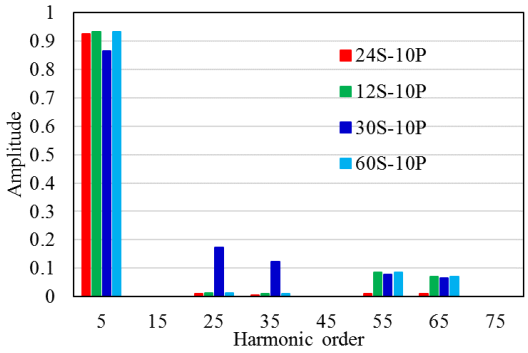

(b) FFT spectrum comparison

Fig. 2. Four PMaSynRM with different winding topologies.

From (12), only MMF harmonics with orders of $(6k\pm1)P$ contribute to torque ripple. Thus, both 25th and 35th MMF harmonic contribute to 6th order torque ripple, and both 55th and 65th contribute to the 12th order torque ripple.

As can be seen from Fig. 2, for 24S-10P, all the torque-ripple-producing stator MMF harmonics including 25th, 35th, 55th and 65th are significantly reduced. The 12S-10P features reduced harmonics of 25th and 35th contributing to 6th order torque ripple. The high torque-ripple-producing stator MMF harmonics contributing to 6th and 12th order torque ripple exhibit in the 30S-10P case. However, for 60S-10P, only the torque-ripple-producing stator MMF harmonics contributing to 12th order torque ripple exhibit.

B. Rotor MMF Harmonics

Based on field-modulating theory [14], the rotor space MMF harmonics after interacting with the stator teeth can be achieved [15].

For the 24S-10P motor, the rotor MMF harmonics are $(2k\pm1)*5$ and $24k\pm5$. Similarly, all the rotor MMF harmonics can be summarized in TABLE II.

TABLE II
ROTOR MMF HARMONICS FOR DIFFERENT SLOT-POLE COMBINATIONS

Slot-pole	Harmonics	Harmonics with considerable amplitude
24S-10P	(2k±1)*5	5, 15, 25, 35, 55, 65
	24k±5,	(19, 29), (43, 53), (67, 77)
12S-10P	(2k±1)*5	5, 15, 25, 35, 55, 65
	12k±5,	(7, 17), (19, 29), (31, 41)
30S-10P	(2k±1)*5	5, 15, 25, 35, 55, 65
	30k±5, 30k±15	(25, 35), (55, 65), (85, 95), (45, 75)
60S-10P	(2k±1)*5	5, 15, 25, 35, 55, 65
	60k±5, 60k±15	(55, 65), (115, 125), (175, 185), (45, 75)

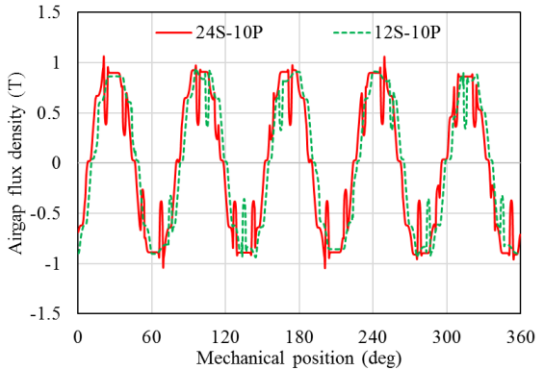

(a) Airgap flux density for 24S-10P and 12S-10P

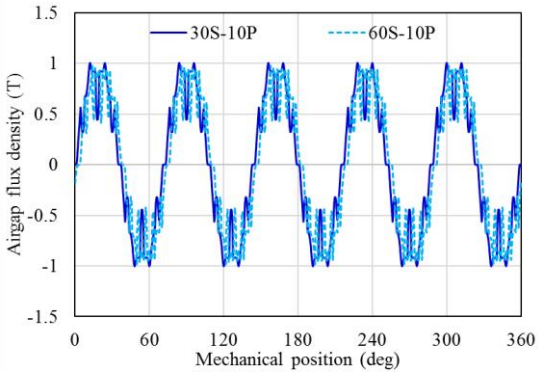

(b) Airgap flux density for 30S-10P and 60S-10P

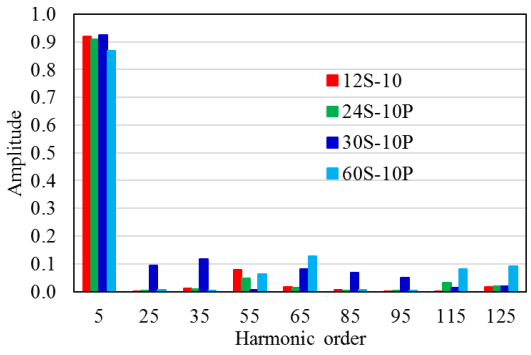

(c) FFT spectrum comparison

Fig. 3. Airgap flux density of the PMaSynRM with different winding topologies.

Generally, the amplitude of the first or second group of slot harmonics for the rotor fundamental MMF harmonic is considerable. It is worth noting that for the winding configurations where q is fractional, viz., 24S-10P and 12S-10P, the order of those slot harmonics corresponding to the rotor fundamental harmonic do not meet the requirement of $(6k\pm1)P$. Hence, although their amplitude is considerable, they do not generate torque ripple from (12).

For the winding configurations where q is integer, viz., 30S-10P and 60S-10P, the order of those slot harmonics corresponding to the rotor fundamental harmonic meet the requirement of $(6k\pm1)P$. Thus, those slot harmonics will generate significant torque ripple due to their considerable amplitude from (12).

Since analytically predicting the rotor MMF harmonic is not the main purpose of this paper, the airgap flux density under no-load condition of these four winding topologies (slot-pole combinations) is simulated as an index of rotor MMF harmonics using an FEA program, as shown in Fig. 3. Again, only those harmonics with order of $k*P$ have been plotted. The impact of stator and rotor MMF harmonics will be discussed in the next section.

C. Torque Ripple Characteristics

After analyzing the harmonic distribution of both the stator and rotor MMF harmonics, the relative amplitude of torque-ripple-producing harmonics such as $5*P$ and $7*P$, $11*P$ and $13*P$ can be observed. Based on the torque ripple expression of (12), the torque ripple characteristics can be evaluated.

As can be seen, for 30S-10P case, the 25th and 35th, 55th and 65th, 85th and 95th harmonic exist in both stator and rotor MMF harmonics. Thus, 6th, 12th, and 18th order torque ripple is expected. For the 60S-10P case, only 12th and 18th order torque ripple exist as the space harmonics corresponding to 6th torque ripple are eliminated in both stator and rotor MMF.

For the winding configurations where q is fractional, viz., 24S-10P and 12S-10P, the 25th and 35th, and 55th and 65th are considerably reduced at varying extent. Therefore, a lower torque ripple can be expected.

Lastly, among all of them, the proposed 24S-10P PMaSynRM features the lowest torque-ripple-producing space harmonics. Therefore, it has the lowest torque ripple. The FE verification will be presented later.

IV. FE Verification

In this section, the EM performance of these four motors will be studied using an FEA program and compared. To make a fair comparison, both the rotor and turns per phase in series are kept the same and only stator numbers are changed. TABLE III summarizes the main geometry of the motor.

A. No-load Performance

The cogging torque waveform of the four motors is calculated and plotted in Fig. 4. As can be seen, the winding configurations where q is fractional such as 24S-10P and 12S-10P feature a much lower cogging torque than the ISDW cases such as 30S-10P and 60S-10P. This is reasonable as the cogging torque is determined by the least common multiplies (LCM) of the slot-pole combination. The higher the LCM, the lower the cogging torque [16].

TABLE III
Main Geometry of the Four PMaSynRMs with Different Winding Topologies

Parameter	Data	Parameter	Data
Stator outer diameter (mm)	200	Stator core	JN270-35
Stator inner diameter (mm)	121.6	Rotor core	JN270-35
Stack length (mm)	40	Magnet material	Sm2Co17
Airgap length (mm)	0.8	Peak current (A)	50
Based speed (rpm)	1910	Rated current (A)	25

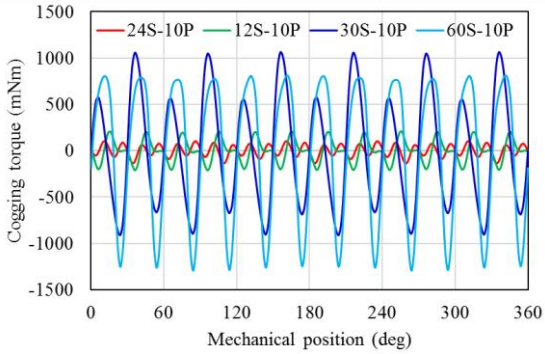

Fig. 4. Comparison of cogging torque.

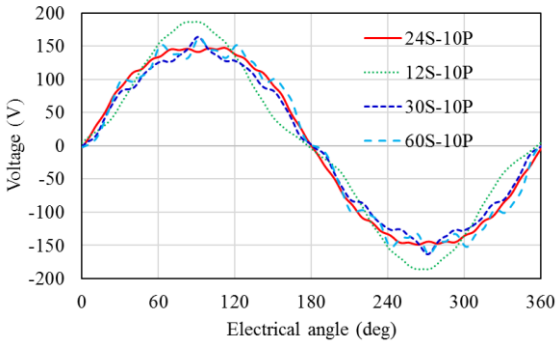

(a) Back EMF waveform

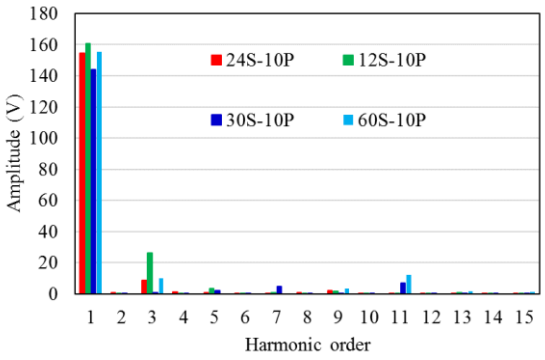

(b) FFT spectrum comparison

Fig. 5. Comparison of no-load back EMF @1910 rpm.

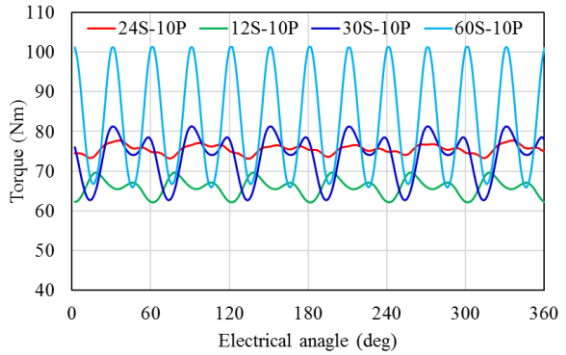

(a) EM torque waveform

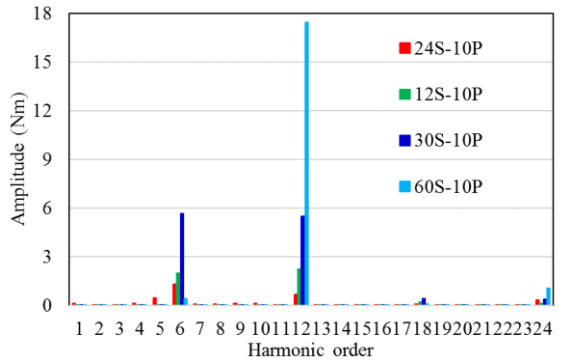

(b) Harmonic distribution of EM torque

Fig. 6. EM torque under MTPA operation with peak current.

The no-load back EMF of the four motors at base speed of 1910rpm is calculated and plotted in Fig. 5. Their back EMF waveform is not purely sinusoidal. An FFT spectrum shows that the relative magnitude of the fundamental EMF harmonic for the four motors is in accordance with their winding factors as developed in TABLE I.

The 24S-10P features minimum harmonic content. The torque-ripple-producing EMF harmonics such as 5th and 7th, and 11th and 13th are significantly reduced. The 12S-10P is similar to the 24S-10P but exhibits a higher 3rd and 5th EMF harmonic. However, the torque-ripple-producing EMF harmonics are rich in both 30S-10P and 60S-10P. Thus, the lowest torque ripple again is expected for the proposed 24S-10P motor.

B. Load Performance

The EM torque waveform of the four motors under peak current with maximum torque per ampere (MTPA) operation is plotted in Fig. 6. Their average value and torque ripple are summarized in TABLE IV.

The 12S-10P PMaSynRM has the lowest average torque of 66Nm, which is because of their reduced reluctance torque capability [7]. The proposed 24S-10P PMaSynRM has slightly higher average torque than the 30S-10P, but a lower torque than the 60S-10P.

The lowest torque ripple of 6% is observed for proposed 24S-10P PMaSynRM. The 12S-10P PMaSynRM has a slightly higher torque ripple of 12%. Much higher torque ripple is seen for both 30S-10P and 60S-10P. The significant torque ripple for 60S-10P is due to the fact that the lowest order of its torque ripple harmonic is 12, and from (12) the high order space harmonic may contribute disproportionally to the torque ripple amplitude.

TABLE IV
EM TORQUE OF THE FOUR PMASYNRMS UNDER MTPA OPERATION WITH PEAK CURRENT

	24S-10P	12S-10P	30S-10P	60S-10P
MTPA angle (deg)	30	45	50	50
Average torque (Nm)	75.6	66.0	73.8	83.0
Peak to peak torque (Nm)	4.7	7.6	18.6	35.3
Torque ripple (%)	6	12	25	42

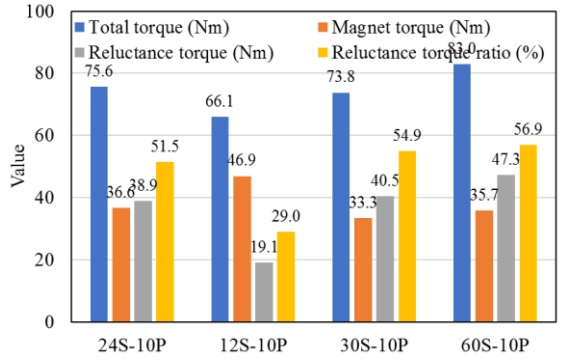

Fig. 7. Torque components under MTPA operation with peak current.

Fig. 7 shows the torque components of the four PMaSynRMs under MTPA operation with peak current. The reluctance torque contribution of the proposed 24S-10P PMaSynRM is 51.5% which is very close to the 30S-10P and 60S-10P. For the 12S-10P PMaSynRM, the reluctance torque ratio is very limited, about 29%.

All this confirms that the proposed 24S-10P features much lower torque ripple while keeping a good reluctance torque capability.

C. Inductance Analysis

The inductance value of each component is calculated and summarized in TABLE V, where L_0, M_0, L_2, and M_2 are directly calculated from FE analysis.

TABLE V
COMPARISON OF INDUCTANCE COMPONENTS

	24S-10P	12S-10P	30S-10P	60S-10P
L_0	6.9	9.2	4.3	5.3
M_0	-1.5	-0.4	-2.0	-2.0
L_2	-1.7	-2.8	-1.2	-1.5
M_2	-1.4	-0.4	-1.2	-1.5
Mutual inductance factor (M_2/L_2)	0.80	0.12	1.00	1.00
L_d	6.2	7.8	4.5	5.0
L_q	10.7	11.3	8.2	9.6
Saliency ratio	1.7	1.5	1.8	1.9

As can be seen, the conventional 12S-10P has a negligible mutual inductance between phases while the proposed 24S-10P features a much higher mutual inductance. The mutual inductance ratio comparison shows that the proposed 24S-10P has a comparable mutual coupling between phases compared to the conventional ISDW cases i.e. 30S-10P and 60S-10P. A comparable saliency ratio compared to conventional ISDW cases is

also observed in the proposed 24S-10P PMaSynRM.

In addition, this reveals that one of the key ways to improve the reluctance torque is to enhance the mutual coupling between phases; and this is the reason for the improved reluctance torque capability of the proposed 24S-10P PMaSynRM compared to conventional FSCW configurations.

V. CONCLUSIONS

This paper presents a 24 slots 10 poles PMaSynRM, which has a fractional slot distributed winding (FSDW). The stator and rotor space MMF characteristics have been presented to reveal the principle of low torque ripple. In addition, the mutual inductance ratio is introduced to reveal the essence of improving reluctance torque capability. Compared to PMaSynRM equipped with the conventional ISDW, the proposed 24 slots 10 poles PMaSynRM has the advantages of much lower cogging torque and torque ripple while keeping a comparable reluctance torque capability. All this demonstrates it could be a good trade-off solution for traction motor application. More studies on the performance such as efficiency and demagnetization characteristics over a wide range speed operation and experimental validation will be reported in future publications.

REFERENCES

[1] Jurkovic, Sinisa, et al, "Next generation chevy volt electric machines; design, optimization and control for performance and rare-earth mitigation." 2015 IEEE Energy Conversion Congress and Exposition (ECCE), pp. 5219-5226, 2015.

[2] Dorrell, David G., et al. "Comparison of different motor design drives for hybrid electric vehicles." 2010 IEEE Energy Conversion Congress and Exposition (ECCE), 2010, pp. 3352-3359.

[3] Boldea, I., Tutelea, L.N., Parsa, L. and Dorrell, D., "Automotive electric propulsion systems with reduced or no permanent magnets: An overview." IEEE Trans. Ind. Electron., vol. 61, no.10, pp.5696-5711, 2014.

[4] Zhu, S., Cox, T., Xu, Z. and Gerada, C., "Novel 24-slots14-poles fractional-slot concentrated winding topology with low-space harmonics for electrical motor." The Journal of Engineering, 2019(17), pp.3784-3788.

[5] Sarlioglu, B., Morris, C.T., Han, D. and Li, S., "Benchmarking of electric and hybrid vehicle electric motors, power electronics, and batteries." 2015 International Conference on Optimization of Electrical & Electronic Equipment (OPTIM), pp. 519-526. IEEE, 2015.

[6] Dajaku, G.; Gerling, D., "A Novel 24-Slots/10-Poles Winding Topology for Electric motors." 2011 IEEE International Electric Motors & Drives Conference (IEMDC), pp.65-70, 2011.

[7] M. Gamba, G. Pellegrino and A. Vagati, "A new PM-assisted Synchronous Reluctance machine with a nonconventional fractional slot per pole combination." 2014 International Conference on Optimization of Electrical and Electronic Equipment (OPTIM), pp. 268-275, 2014.

[8] Thomas A. Lipo, Introduction to AC Machine Design. Wiley-IEEE Press, 2018.

[9] Ge, Hao, "Fractional slot concentrated winding interior permanent magnet motors with reluctance torque: inductance-based methodology for comprehensive analysis, design, and control." PhD dissertation, 2016.

[10] Gamba, Matteo, et al, "Synchronous reluctance motor with concentrated windings for IE4 efficiency." 2017 IEEE Energy Conversion Congress and Exposition (ECCE). IEEE, pp. 3905-3912, 2017.

[11] Han, Seok-Hee, Thomas M. Jahns, and Wen L. Soong, "Torque ripple reduction in interior permanent magnet synchronous machines using the principle of mutual harmonics exclusion." 2007 IEEE Industry Applications Annual Meeting, pp. 558-565, 2007.

[12] L. Alberti, M. Barcaro and N. Bianchi, "Design of a Low-Torque-Ripple Fractional-Slot Interior Permanent-Magnet Motor." IEEE Trans. Ind. App., vol. 50, no. 3, pp. 1801-1808, 2014.

[13] Vagati, Alfredo, et al., "Design of low-torque-ripple synchronous reluctance motors." IEEE Trans. Ind. App., vol. 34, no. 4, pp. 758-765, 1998.

[14] M. Cheng, P. Han and W. Hua, "General Airgap Field Modulation Theory for Electrical Machines." in IEEE IEEE Trans. Ind. Electron., vol. 64, no. 8, pp. 6063-6074, 2017.

[15] N. Bianchi, M. D. Pré, G. Grezzani, and S. Bolognani, "Design considerations on fractional-slot fault-tolerant synchronous motors," IEEE Trans. Ind. Appl., vol. 42, no. 4, pp. 997-1006, 2006.

[16] Bianchi, N. and Bolognani, S., "Design techniques for reducing the cogging torque in surface-mounted PM motors." IEEE Trans. Ind. App., vol. 38, no. 5, pp.1259-1265, 2002.